Supplementary Materials: Discriminating High-Pressure Water Phases Using Rare-Event Determined Ionic Dynamical Properties

Lin Zhuang(庄琳)[1,2], Qijun Ye(叶麒俊)[1,2], Ding Pan(潘鼎)[3,4], and Xin-Zheng Li(李新征)[1,2,5]

[1]Institute of Condensed Matter and Material Physics, School of Physics, Peking University, Beijing 100871

[2]State Key Laboratory for Artificial Microstructure and Mesoscopic Physics, Frontier Science Center for Nano-optoelectronics and School of Physics, Peking University, Beijing 100871

[3]Department of Physics and Department of Chemistry, Hong Kong University of Science and Technology, Hong Kong

[4]HKUST Fok Ying Tung Research Institute, Guangzhou 511458

[5]Collaborative Innovation Center of Quantum Matter, Peking University, Beijing 100871

1 OUTLINE

In the main text, we show the dynamic feature determined phases and the overall phase diagram of high-pressure water. In this supplementary material, we discuss the reliability of these simulations and the criteria from which these conclusions are drawn as well as some computational details. We firstly show the convergence test of the supercell size, see Fig. S1. The accuracy of trained potential can be perceived by the almost merged radial distribution functions (RDFs) to the DFT ones, as shown for more (T, P) configurations in Fig. S2. We showed the diffusion coefficients and the corresponding MSDs at more pressures in Fig. S3 and Fig. S4, respectively. For the distribution of protons' displacements, we show two different converge tendencies in Δt in Fig. S5. The distribution details for static ice VII and dynamic ice VII are shown in Fig. S6 and Fig. S7, correspondingly. In Fig. S8, we show the fitting results of Burr distribution and normal distribution to the lineshape of the distribution of protons' displacements. We also give the lifetime distribution of OH^-, O^{2-}, H_3O^+ and H_2O species in superionic ice (SI), see Fig. S9. The two-phase method was used as the benchmark for determining the phase boundary, by eliminating the hysteresis effect. We show its implementation scheme and the corresponding results, in Fig. S10 and Fig. S11. Finally, based on the criterion of above dynamic features, we distinguish several novel phases within the acknowledged phases. We list all the l_as mentioned in Fig. 3c of main manuscript, see TABLE S1. These phases are well-defined by their individual dynamic features, as summarized in TABLE S2.

2 Simulation Details: Training Set and Molecular Dynamics

As the input data for the NN potential, we use Vienna *ab initio* Simulation Package (VASP) to run a series of MD simulations with T (P) ranging from 300 to 3,000 K (5 to 70 GPa). For phases at low Ts, which are out of the range of this study, strong nuclear quantum effects should be important and one should resort to a combination of path-integral based methods. The calculated configurations are selected to be representative for all involved phases in the P-T region of interest, including ice VII, superionic ice and liquids of different forms. For each DFT simulation, we run 2.5-10 ps MD simulation with 0.5 fs time step, ensuring quasi-ergodicity and sufficient sampling. To describe Van der Waals (vdW) interactions, the strongly constrained and appropriately normed (SCAN) functional was used, which outperforms others functionals with comparable computational cost in similar water systems. The energy cutoff of the plane-augment wave (PAW) is set as 900 eV.

Upon deriving the NN potential, the MD simulations with NN potential are then preformed by Large-scale Atomic/Molecular Massively Parallel Simulator (Lammps) with DeePMD module. For each (P, T) configuration, NPT simulations (up to 50 ps) are preliminarily performed to derive the equilibrium volume, and long time NVT simulations (up to 0.5 ns) with this volume and Nosé-Hoover thermostat are then performed. A 4×4×4 supercell containing 128 water molecule is used in above simulations (for the convergence test, see next section).

3 Convergence Test of Supercell Size

In order to alleviate the size effect, we make the convergence test of supercell size. In Fig. S1, we check the dependencies of density and potential energy on the cell size in the MD simulations using cells containing 2, 16, 128, 432 and 1024 water molecules. Consistent with previous literature, simulation cell with 128 water molecule is able to provide converged results. We use this $4 \times 4 \times 4$ supercell (with 128 water molecule) thorough our simulations.

4 Radial Distribution Functions

Based on the NN potential results, we plot the RDFs at other (T, P) configurations. The accuracy of trained potential can be perceived by the almost merged RDFs to DFT ones, as shown for more (T, P) configurations in Fig. S2.

5 Diffusion Coefficients and Mean Square Displacement

We show the diffusion coefficients and mean square displacement at different temperatures and pressures. All of these diffusion coefficients are derived from the corresponding long-time behavior of mean square displacement. At 5 GPa, the static ice VII directly melts into molecular liquid and stays at such condition at 10 GPa. When pressure goes up to 40 GPa, there are additionally superionic ice and SI′ phases. The varying pattern of D_{O} and D_{H} curves in 70 GPa is the same as the ones of in 60 GPa, which we have discussed in details in the main text.

As mentioned in the main text, the diffusion coefficients are inappropriate for low temperature region. We notice the nontrivial MSD curves of protons in this region. Instead of the regular linear lineshape of MSD in the long time limit for liquid (with finite slope) and solid (horizontal), there are several plateaus arising randomly in the MSD curves of this region. With higher temperature, the plateaus appear more frequently, and finally merge into the linear lineshape in the liquid region. The plateaus mean the protons are bounded in local minimums of the potential energy surface for a certain time before they escape, i.e. the proton transfers are rare events. We show the MSD curves at 10, 20, 30, 40, 50, 60 and 70 GPa, respectively.

6 The Distribution of Protons' Displacement

In order to explore the phases in region A and B as mentioned in the main text, we resort to the distribution of atomic displacements. In Fig. S5, we show two different situations, with one can be converged in some value of Δts and the other cannot be converged. Two examples at high (1,400 K) and low (800 K) temperatures at 60 GPa are given. At 800 K, the lineshape is concentrated and $\Delta t = 0.1$ ps is enough to obtain the converged lineshape. While at 1,400 K, there are translational and rotational transfer in H_2O. The distribution of atomic displacement will continue expanding to farther Δr with increasing Δt. We can tell this case apart the converged one by using a long Δt (note the lineshape can vary with different Δt). 0.4 ps seems enough for this purpose and we use this value in the following calculations.

When Δt is vanishingly short, Δr is trivial and linear in velocity, and $P_{\Delta t}(\Delta r)$ follows the Maxwell velocity distribution, see the cases with small Δt in Fig. S6. For more temperatures, the results are shown in Fig. S7. The single peak at low Ts means that protons are localized in the deeper minimum and the shoulder at moderate Ts means that the proton can occasionally transfer to the shallower local minimum along a specific hydrogen bond. When the peaks are inconspicuous at high Ts, it means a combination of translational and rotational transfer and the protons can freely diffuse in the HB network. Based on the displacements at different temperatures, we distinguish the dynamic ice VII into dynamic ice VII T and dynamic ice VII R.

7 The Lifetime of Ions in SI

In Fig. S9, we show the lifetime distribution of OH^-, O^{2-}, H_3O^+ and H_2O. We use the last 10,000 steps of aforementioned simulations, namely 5 ps trajectory, to show the dissociation of H_2O. Geometric criteria, *i.e.* comparing the distance between oxygens and protons with the length of covalent bonding length, is used to determine the binding conditions. At 60 GPa and 2,000 K (or 40 GPa and 1,500 K), H_3O^+ can only exist for very short time, which agrees with the experiments we mentioned in the main manuscript. The majority of conductive ions are OH^- and corresponded H^+.

8 Two-Phase Method

As a benchmark for phase boundary by eliminating the hysteresis effect, two-phase method are also used to obtain the melting line of ice VII and SI. In Fig. S10, we show the implementation scheme. The simulation starts with a coexistence state of solid and liquid (Fig. S10A). Molecular dynamics are performed to reach

the equilibrium: at 10 GPa, for T $\geq$ 700 K, the system transforms into a liquid state (Fig. S10B), whereas for T $\leq$ 650 K, it ends up as solid (Fig. S10C). To determine whether the crystal is melted, we used radial distribution function and MSD, see Fig. S10D and S10E. In Fig. S11, we show the melting line of ice VII and SI and the triangles are the results from two-phase method. The red (blue) triangles are shown for the greatest lower bound of liquid (the least upper bound of solid). The black dash line is the result from main manuscript. It should be noted that the latter half of the dash line is the phase boundary of SI and SI′, not the one of SI′ and ionic liquid. It is because in SI′ the sublattice of oxygens has began to melt, which could be viewed from the liquid-like RDFs. Comparing these two results, we find the hysteresis effect is considered negligible to the phase boundary in our cases, by posing an error of 50 K in our two-phase MD simulations.

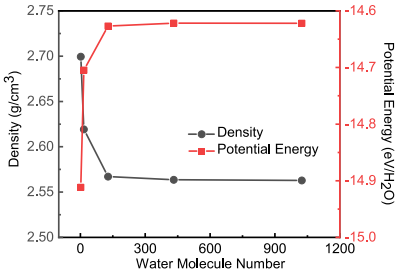

FIG. S1: The size effect on density and potential energy. The black circles indicate the density and red squares indicate the potential energy.

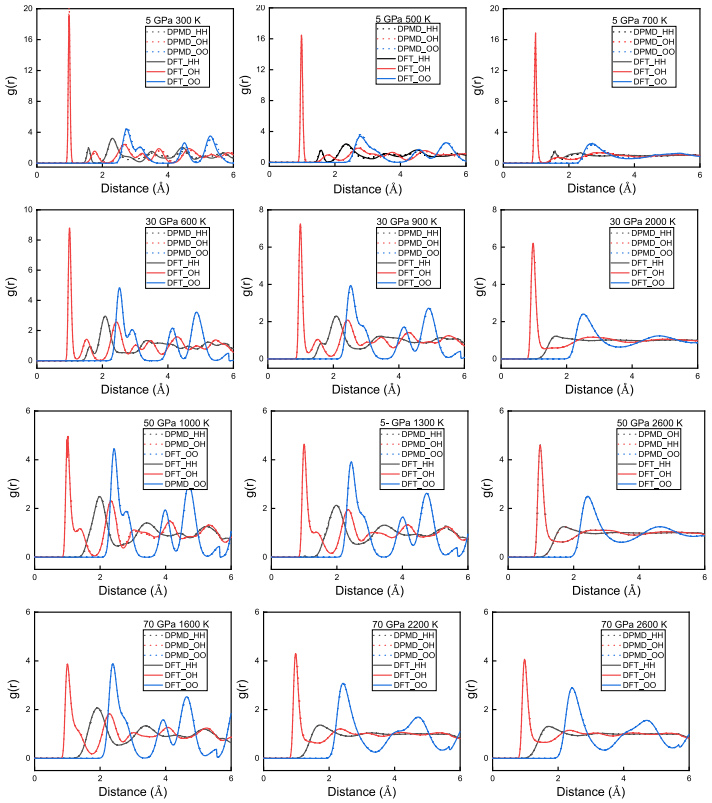

FIG. S2: The RDFs via NN potential and DFT at more (T, P) configurations.

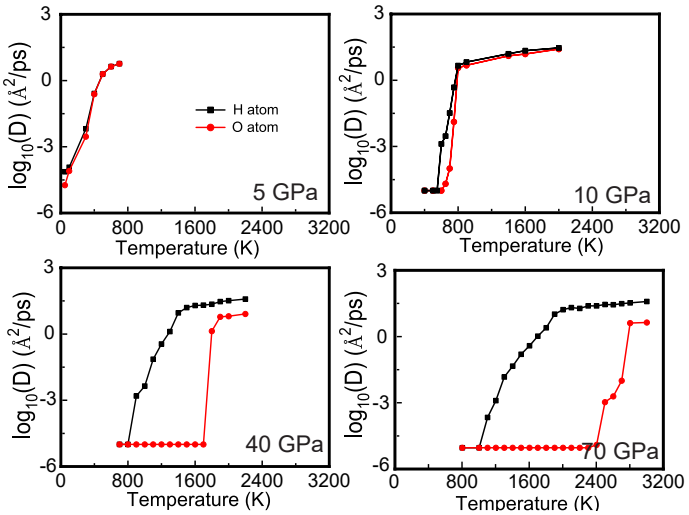

FIG. S3: The D_H and D_O at more (T, P) configurations.

Pressure (GPa)	20	25	30	35	40	50	60
l_a (Å)	3.01	2.96	2.93	2.89	2.86	2.81	2.78

TABLE S1: This table lists all the l_as mentioned in Fig. 3c of main manuscript.

D_O	D_H	$P_{\Delta t}(\Delta r)$	Phases
Negligibly small	Negligibly small	Concentrated, single-peaked	Static ice VII
Negligibly small	Negligibly small	Concentrated peak with a shoulder	dynamic ice VII T
Negligibly small	Increasing with T, but not saturated		
Negligibly small	Increasing with T, but not saturated	Unconcentrated two peaks, and protons begin to diffuse among the lattice	dynamic ice VII R
Negligibly small	Increasing with T and saturated	Inconspicuous peak	Superionic ice
Increasing with T, but not saturated	Increasing with T and saturated	-	SI′
Increasing with T, and the ratio keeps closed to 1		-	ML
Increasing with T, and saturated gradually		-	IL

TABLE S2: The table of all the phases and the dynamic features of them.

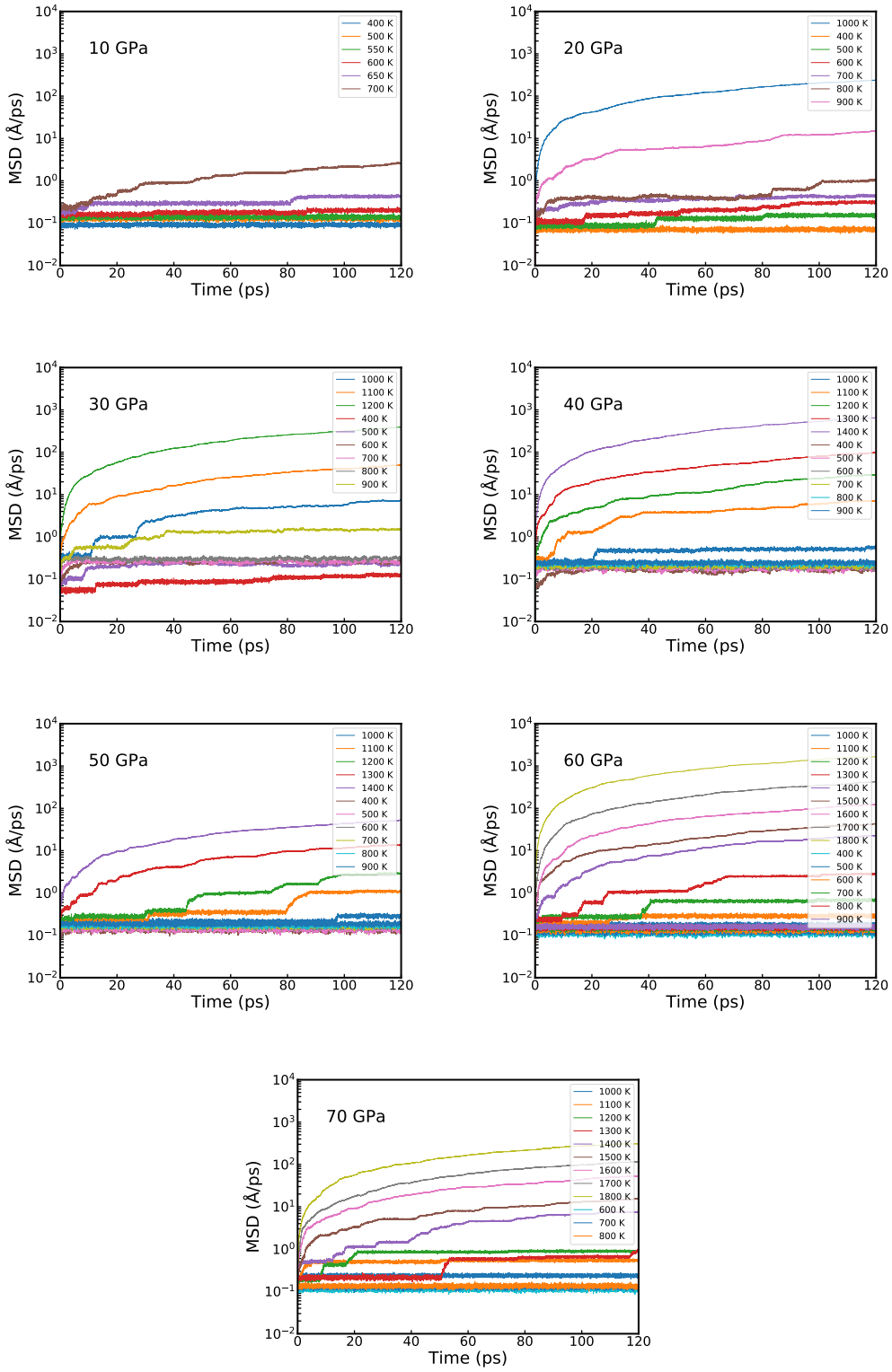

FIG. S4: The MSD of protons at more (T, P) configurations.

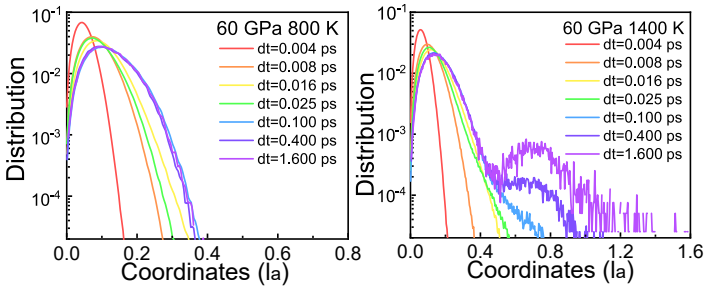

FIG. S5: The distribution of protons' displacement. 800 K and 1,400 K show two different converge tendency in Δt.

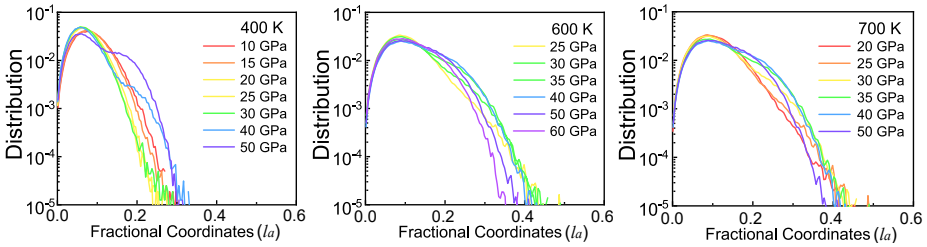

FIG. S6: The distribution of atomic displacements at relatively low temperatures.

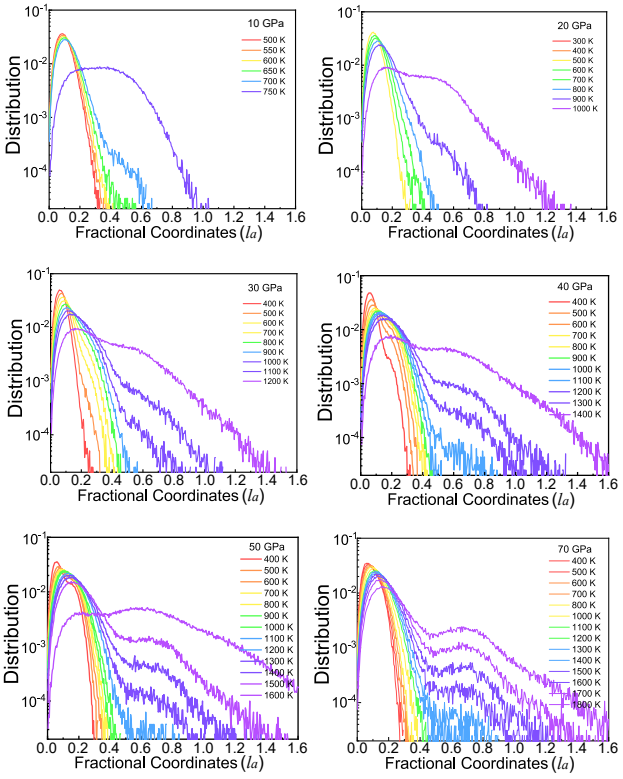

FIG. S7: The distribution of protons' displacements at more (T, P) configurations.

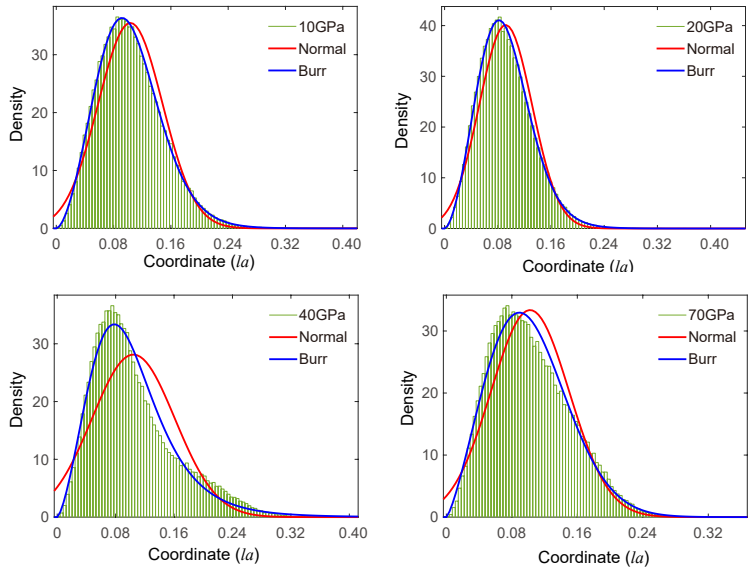

FIG. S8: The fitting result to the lineshape of distribution of protons' displacement. The distribution of static ice VII (only local motions, protons are localized to one covalent site) is well-fitted by Burr distribution. While in the dynamic ice VII T phase (with translational transfer, protons are localized in the oxygen pairs), the distribution cannot be well-fitted. Normal distribution fitting curves are shown for comparisons.

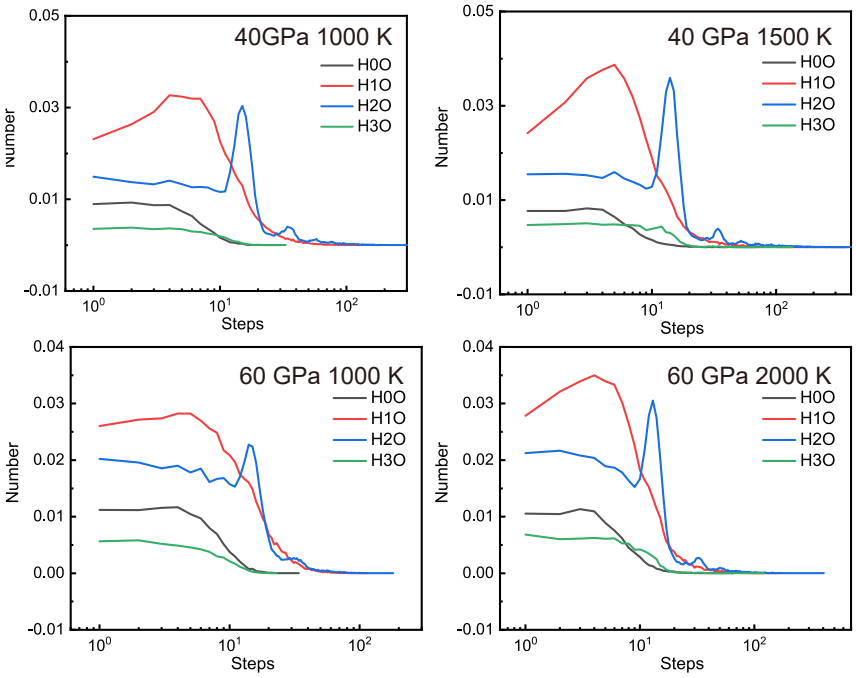

FIG. S9: The lifetime distribution of OH^-, O^{2-}, H_3O^+ and H_2O. The black lines represent for the O^{2-} ions, the red ones for OH^-, the blue ones for H_2O and the green one for H_3O^+.

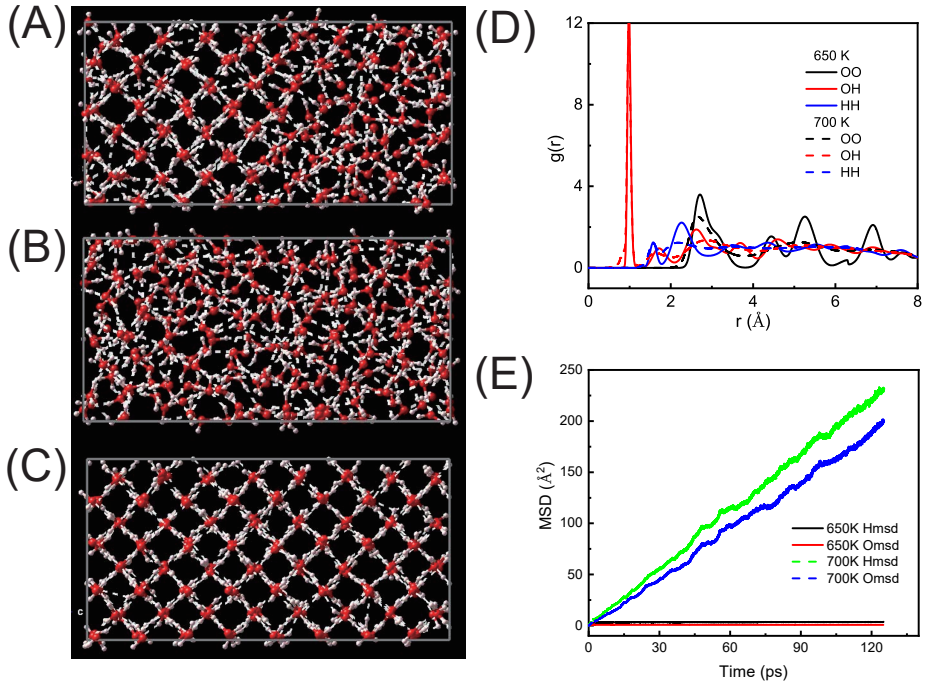

FIG. S10: Two-phase MD simulations. Snapshots of the simulations at 10 GPa showing (A) the starting structure, (B) the final state at 700 K and (C) the final state at 650 K. (D) The radial distribution function g(r) at 650 K and 700 K. At 650 K, the solid state persists (solid lines) as indicated by the relatively sharp peaks. At 700 K (bash lines), these peaks are much broader and the g(r) is characteristic of a liquid. (E) The MSDs as a function of time.

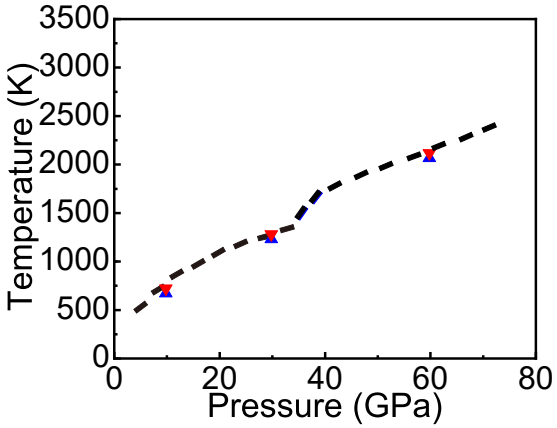

FIG. S11: The melting line of ice VII and superionic ice. The red and blue triangles indicate the greatest lower bound of liquid and the least upper bound of solid from the two-phase simualtions, respectively.